Int J Fract
https://doi.org/10.1007/s10704-024-00828-w

RESEARCH

Cyclic tearing of a woven fabric embedded in a soft matrix

Jingyuan Tang · Fengkai Liu · Xi Chen · Zhigang Suo · Jingda Tang

Received: 11 July 2024 / Accepted: 14 October 2024

Abstract A composite of a woven fabric embedded in a soft matrix exhibits the attributes of both constituents. The fabric is strong in tension but flexible in bending. The soft matrix impedes fluid penetration. Applications of such composites include tents, rain coats, and wound closure patches. How such a composite tears under cyclic load remains unclear. Here we embed a woven fabric of ultrahigh molecular weight polyethylene in a soft matrix of thermoplastic polyurethane, and tear each specimen of the composite with cyclic energy release rate of a fixed amplitude, G. Two thresholds are identified, G_a and G_b. When $G < G_a$, the composite does not tear. When $G_a < G < G_b$, the composite tears by yarn slip without yarn break, and then tearing arrests after yarns jam. When $G_b < G$, the composite tears, without arrest, by a combination of yarn slip and yarn break. We then prepare a composite with strengthened fabric-matrix interface, and find that G_a increases but G_b decreases. We interpret these findings in terms of stress deconcentration along the yarns. It is hoped that this study will aid the development of fatigue-resistant composites.

Keywords Woven fabric · Fatigue crack growth · Fatigue threshold · Soft composite · Crack bridging

1 Introduction

Biological tissues, such as tendon and cartilage, are composites of strong collagen fibers and soft matrix of proteoglycan and glycosaminoglycans (Vesely 1997; Szczesny et al. 2017). Such biological tissues have remarkable mechanical properties, including high strength, high toughness, and high fatigue resistance. For instance, the tendon has a strength of $\sim$ 100 MPa (Sharabi 2022). The bovine pericardium has a toughness of 15 kJ/m^2 and a fatigue threshold of 4.3 kJ/m^2 (Zeng et al. 2023).

Synthetic materials have been developed to mimic the fiber-matrix structure of biological tissues, and reproduce their outstanding mechanical properties (Liao et al. 2013; Wang et al. 2019; Li et al. 2020a; Xiang et al. 2020; Yang et al. 2021; Zhang et al. 2021; Liu et al. 2022b). Among these materials is a class of composites of plain woven fabrics embedded in soft matrices (King et al. 2015; Huang et al. 2017, 2019). Such a composite exhibits the attributes of both

J. Tang · F. Liu · X. Chen · J. Tang (✉)
State Key Laboratory for Strength and Vibration of Mechanical Structures, Department of Engineering Mechanics, Xi'an Jiaotong University, Xi'an 710049, China
e-mail: tangjd@mail.xjtu.edu.cn

Z. Suo
John A. Paulson School of Engineering and Applied Sciences, Kavli Institute for Bionano Science and Technology, Harvard University, Cambridge, MA, USA

Published online: 08 January 2025

constituents. The fabric is strong in tension but flexible in bending. The soft matrix impedes fluid penetration (Patti et al. 2021). Applications of such composites include tents, raincoats, and wound closure patches. Recently, the composite composed of woven fabric and soft matrix has been proposed as a potential material for mimicking biological tissues such as tendon and cartilage. This soft composite shows extraordinarily high tearing strength and toughness, which depends on the modulus ratio of matrix and fiber, the interface strength between matrix and fiber, and the work of fracture of both two components (Cui et al. 2020, 2021). The tensile property of the composite without precuts has been studied under cyclic load (He et al. 2022). However, we are unable to identify any published work on cyclic tearing of a woven fabric embedded in a soft matrix.

In retrospect, the composites of woven fabric and rigid matrix haven been widely used in automobiles, and aerospace, because of their light weight and outstanding mechanical properties (Kumar et al. 2018). Commonly used fabric types include Kevlar fabric, polyethylene fabric, glass fabric, carbon fabric, etc. (Rajak et al. 2022). The fracture and fatigue properties of the woven fabric itself have also been studied for decades. For woven fabric, the tearing strength is measured by the trousers tearing test (Taylor 1959). The tear strength and tear energy of fabrics under monotonic loading are governed by the slip force between yarns and the strength of the yarns (Triki et al. 2011, 2012). Cyclic loading makes the tear resistance of fabrics lower than that in monotonic loading (Liu et al. 2022a). The rigid composites are usually manufactured in the form of laminates, and their strength, stiffness, impact resistance and prediction of the fatigue life have been well investigated (Kim and Sham 2000; Pandita et al. 2001; Bresciani et al. 2015; Sevenois and Van Paepegem 2015; Ghanavaty et al. 2024).

Here we embed a woven fabric of ultrahigh molecular weight polyethylene (UHMWPE) in a soft matrix of thermoplastic polyurethane (TPU). We tear each specimen under cyclic energy release rate of a fixed amplitude, G. Two thresholds are identified, G_a and G_b. When $G < G_a$, the crack does not propagate. When $G_a < G < G_b$, the crack initially propagates in the matrix and eventually arrests with no yarn break. When $G > G_b$, the yarns at the crack tip break and the crack propagates continuously. We further strengthen the interface by diluting the solution of TPU and plasma treatment of the fabric. The composite with a strong interface has an increased G_a, but a decreased G_b. This work may provide insight for designing fatigue-resistant composites.

2 Fabrication of composite

The thermoplastic polyurethane (TPU) particles are purchased from BASF (commercial name: EC 60 A 10 P Elastollan©); Tetrahydrofuran (THF) is purchased from Aladdin; Ultrahigh molecular weight polyethylene (UHMWPE) fabric (Mass per unit area: 33 g/m^2) is purchased from Jiangsu PTC New Material Technology Co., Ltd (Fig. 1d). The fabric is manufactured by fixing a set of yarns in one direction, called the warp direction, and then weaving another set of yarns in the perpendicular direction, called the weft direction. Each yarn consists of 80 fibers. The composite is coated with gold in an ion-sputtering machine (Hitachi MC1000), and then observed in a scanning electron microscope (Hitachi SU3500). The SEM image of the fabric shows the warp yarns and the weft yarns (Fig. 1e).

We mix 20 g of thermoplastic polyurethane (TPU) particles and 180 g of tetrahydrofuran (THF) (Fig. 1a). After the mixture is stirred by a magnetic agitator for 12 h, the TPU particles dissolve in the THF solvent to form a solution (10 wt%). A piece of the UHMWPE fabric (13 cm × 15 cm) is soaked in the solution for 30 min (Fig. 1b), and then hung on an iron support in a fume hood for 12 h to evaporate THF completely (Fig. 1c). The composite is cut with a sharp blade to expose the cross section, and then the cross section is observed in a scanning electron microscope (Fig. 1g). The photo and SEM image show that TPU elastomer embeds the fabric to form a composite (Fig. 1f). The thickness of the composite is 110 ± 20 μm, measured by a screw micrometer. When taking the SEM image of the cross section, the matrix cannot constrain the fibers in the yarn, resulting in a slightly higher thickness of the exposed cross section (Fig. 1g).

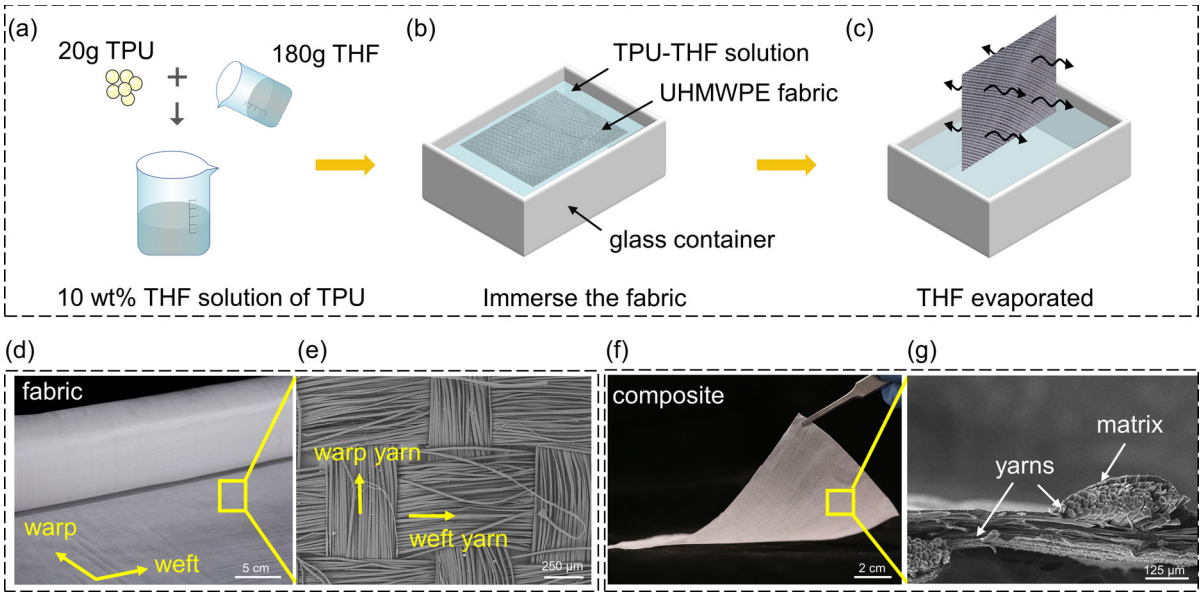

Fig. 1 Fabrication of a composite of woven fabric and soft matrix. **a** Dissolve TPU particles in THF solvent to form a TPU-THF solution. **b** Immerse the polyethylene fabric in the TPU-THF solution. **c** Evaporate THF to form a fabric-elastomer composite. **d** A photo of the woven fabric. **e** A SEM image of the woven fabric. **f** A photo of the composite. **g** A SEM image of the cross section of composite

3 Tearing of the composite under cyclic load

We tear the composite using the trousers specimen. The specimen is cut into a rectangular shape (40 mm × 100 mm × 110 μm) with the long edge in the warp direction. An initial notch (40 mm) is cut by scissors in the middle of the specimen along the warp direction. All the samples in this work have the same geometry and the crack direction are all along the warp direction. The two legs of the specimen are gripped by a universal mechanical test machine (SHIMADZU AGS-X) with a load cell of 1000 N, as shown in the inset of Fig. 2a. When the specimens are cyclically loaded at a prescribed amplitude of force, we record the displacement of the crosshead. For every test in this work, the velocity of the crosshead is set at 50 mm/min during both loading and unloading. There is not any holding period applied at the maximum stress. The minimum force applied is 0 N. The test is terminated at 30,000 cycles. The images of the specimens are recorded using a digital camera (Canon EOS 5D).

We tear a specimen under cyclic force of a low amplitude of 1N. The force–displacement curves at different cycles are recorded (Fig. 2a). The displacement increases sharply in the first 1000 cycles, slows down in the following cycles, and increases negligibly after 10,000 cycles (Fig. 2b). The morphology of the crack tip before and after the test are observed (Fig. 2c). There is no yarn slip or yarn break at the crack tip (Fig. 2d). The displacement is due to the rearrangement of the fibers in the first yarn ahead of the crack tip.

We tear another specimen under cyclic force of an amplitude of 60N. The force–displacement curves at different cycles are recorded (Fig. 3a). The force–displacement hysteresis is large for the first cycle, but is small in later cycles. When $N > 1$, the loading and unloading curves overlap together. The maximum displacement in each cycle increases sharply in the first 5000 cycles, slows down in the following cycles, and increases negligibly after 15,000 cycles (Fig. 3b). The morphology of the crack tip before and after the test are observed (Fig. 3c). There is yarn slip but no yarn break at the crack tip. In the initial cycles, weft yarns near the crack tip slip along the warp yarns, and jam together to form a delta-shaped zone. The crack propagates by yarn slip. As the cycle increases, more and more weft yarns slip along the warp yarns and jam in the delta-shaped zone. The jammed weft yarns apply great friction on the warp yarns, which in turn impede the yarn slip. In this way, the crack is arrested.

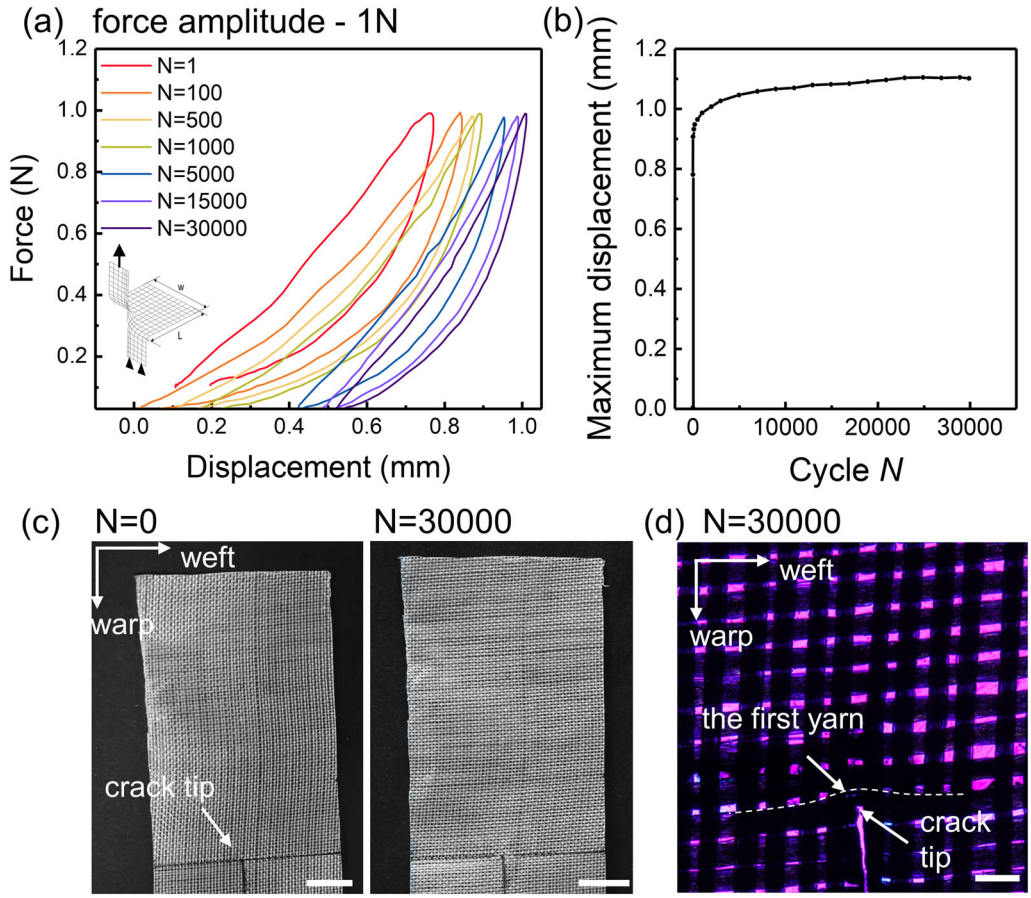

Fig. 2 The composite does not tear under a cyclic force with a low amplitude of 1N. **a** The force–displacement curve over cycles. **b** Maximum displacement as a function of cycle *N*. **c** The crack does not propagate after 30,000 cycles. Scale bar is 10 mm. **d** The micrograph of the crack tip after cyclic loading. Scale bar is 1 mm

The more weft yarns in the delta-shaped zone, the more friction and more difficulty to grow the crack. In fact, it is difficult to observe the crack propagation after 15,000 cycles, and the photos seem the same from the 15,000th to 30,000th cycle.

Next we tear another specimen under cyclic force of an amplitude of 120N. The force–displacement curves at different cycles are recorded (Fig. 4a). When $N > 1$, the loading and unloading curves overlap together. The displacement is plotted as a function of the cycle number (Fig. 4b). The displacement in the first 10,000 cycles is similar to that of low amplitude of force, first growing rapidly and then gradually slowing down. After 10,000 cycles, the displacement profile has changed, showing an increase. We observe the tear process in Fig. 4c. In the first thousands of cycles, the crack propagates by the slip of weft yarns. The weft yarns slip along the warp yarns and form a delta-shaped zone. As the cycle number increases, more and more weft yarns join the delta-shaped zone, and the crack grows slower and slower. After $\sim$ 10,000 cycles, the jammed weft yarns at the crack tip break suddenly. The warp yarns slip and break alternately near the crack tip, so that the crack continues to grow and does not arrest.

We summarize the relation between displacement d and number of cycle N for various amplitudes of cyclic force (Fig. 5a). The force is converted to energy release rate using the formula: $G = 2F/t$, where F is the amplitude of force, and t is the thickness of the specimen (Thomas 1994). Three regimes are observed: yarns neither slip nor break, yarns slip but do not break, and yarns slip and break. The three regimes are demarcated by two thresholds of energy

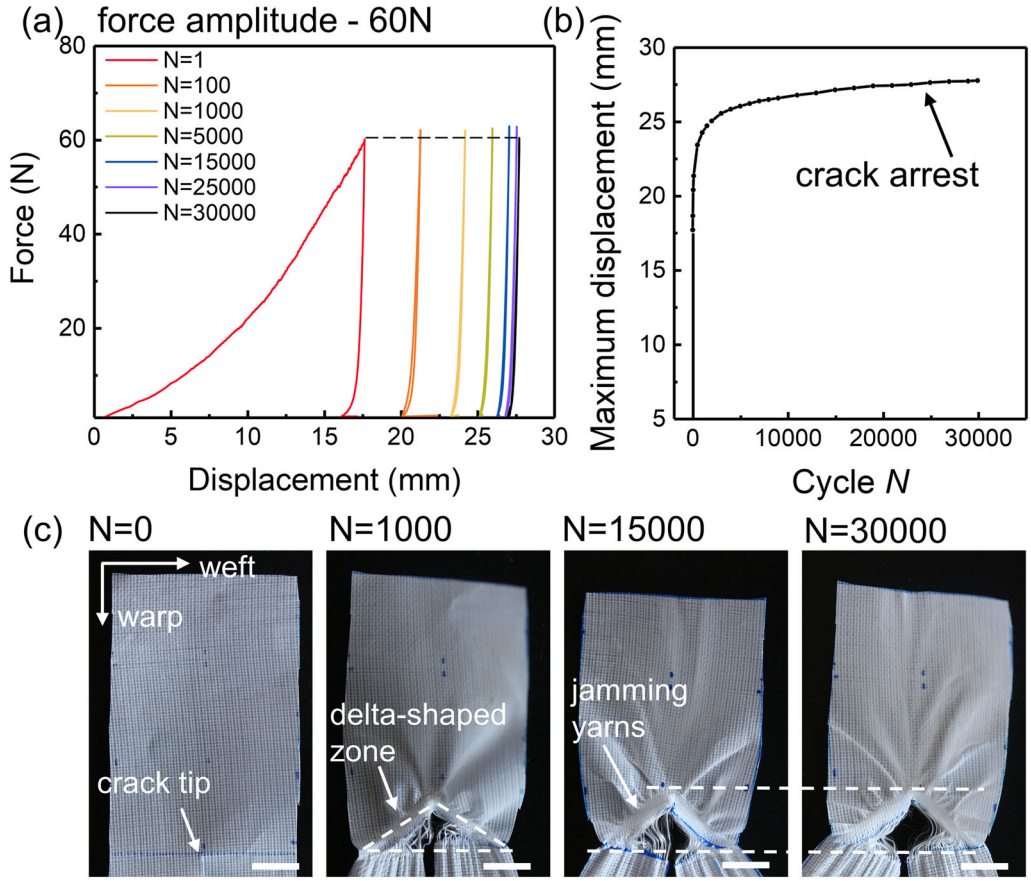

Fig. 3 The composite tears by yarn slip under a cyclic force of an amplitude of 60N. **a** The force–displacement curve over cycles. **b** Maximum displacement as a function of cycle *N*. **c** The crack propagates by yarn slip. Scale bar is 10 mm

release rate, G_a and G_b. When $G < G_a$, the yarns neither slip nor break. When $G_a < G < G_b$, the yarns first slip and jam, but do not break. After initial cycles, the crack arrests. The crack arrest is defined as that the displacement growth per cycle $\Delta d/\Delta N$ is lower than $\sim 10^{-8}$ m/cycle, since the size of the yarns is about $\sim$ 500 μm, and the number of cycles is $\sim$ 10,000. When $G > G_b$, the crack propagates by a combination of yarn slip and yarn break. The final displacement d_f increases with the energy release rate (Fig. 5b). We further plot the displacement per cycle $\Delta d/\Delta N$ as a function of amplitude of energy release rate G (Fig. 5c). When $G > G_b$, the crack propagates continuously, the displacement per cycle $\Delta d/\Delta N$ is calculated as the average displacement per cycle between 5000th and 30,000th cycles. Our test gives the values of the two thresholds: G_a = 15 kJ/m^2 and G_b = 1682 kJ/m^2.

4 Strengthening of the interface between fabric and matrix

When the composite cyclically tears, the yarn slips by the damage of interface between yarns and matrix. The interface strength affects fatigue of the composite. We increase the interface strength by decreasing the concentration of the TPU solution and plasma-treating the fabric surface. We mix 10 g of TPU particles and 190 g of THF. After the mixture is stirred by a magnetic agitator for 12 h, the TPU particles dissolve in the THF solvent to form a dilute solution (5 wt%). Then 40 g of dilute TPU-THF solution is poured into a glass container (19 cm × 14 cm × 4 cm). A piece of UHMWPE fabric (13 cm × 15 cm) is treated by air plasma (Harrick pdc002) for 30 min and then immediately soaked in the TPU-THF solution for 30 min. Then the fabric is kept at the bottom of the container, which is placed in a fume hood with the cover opened

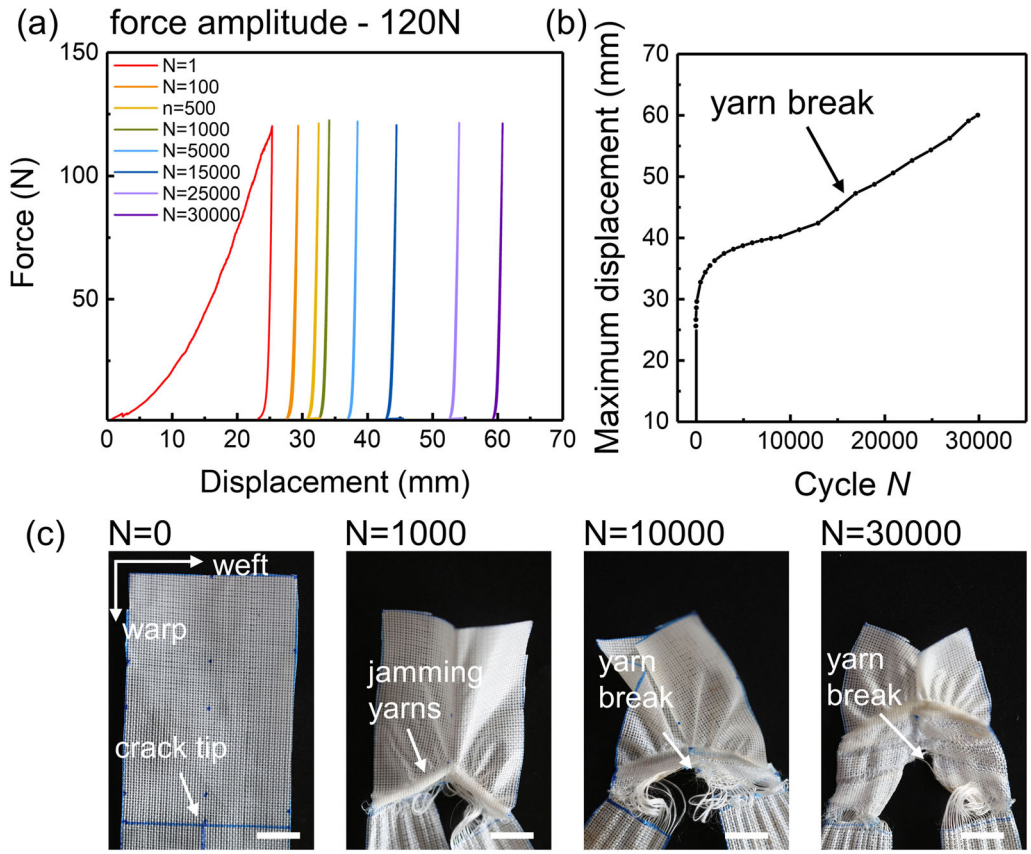

Fig. 4 The composite tears by a combination of yarn slip and yarn break under a cyclic force of a high amplitude of 120N. **a** The force–displacement curve over loading cycles. **b** Maximum displacement as a function of cycle *N*. **c** The crack propagates by yarn break. Scale bar is 10 mm

to evaporate the THF. This composite has a thickness of 110 ± 20 μm.

We use the contact angle test to measure the wettability of the solution and the fabric. The contact angle test is performed on a drop shape analyzer (Kruss DSA100). The drop of liquid is 5 wt% and 10 wt% TPU-THF solution. The drop volume for each test is 2 μL. Without plasma treatment, the contact angle is larger than 30° for both two solutions (Fig. 6a). After plasma treatment, the contact angle decreases to 6° for 5 wt% TPU-THF solution, (Fig. 6b). The SEM images show that the gap between fibers is well infiltrated by the matrix for the composite with a strong interface (Fig. 6c), while gaps exist between fibers for the case of weak interface (Fig. 6d). The 5% TPU-THF solution can better wet the plasma treated fabric.

To compare the interface strength, we pull out single yarns from the two composites, and record the maximum pullout force (Fig. 7a). The specimen is cut into a rectangular shape with a 3 mm width. A warp yarn is selected in the middle of the specimen to be pulled out. The end of this yarn is cut at a location of length measured on the composite. The force–displacement curves are recorded. All tests are repeated three times.

For the same yarn length, the maximum pullout force is larger for the composite with a strong interface than that with a weak interface (Fig. 7a). SEM images show that cohesive failure occurs with matrix residue, when the interface is strong (Fig. 7b), while adhesive failure occurs when the interface is weak (Fig. 7c). The interfacial strength is defined as the peak pullout force per unit contact area between the matrix and the yarn, which is 0.78 MPa for the weak interface and 1.2 MPa for the strong interface.

We tear these two composites monotonically, and record the force–displacement curves (Fig. 8a). The

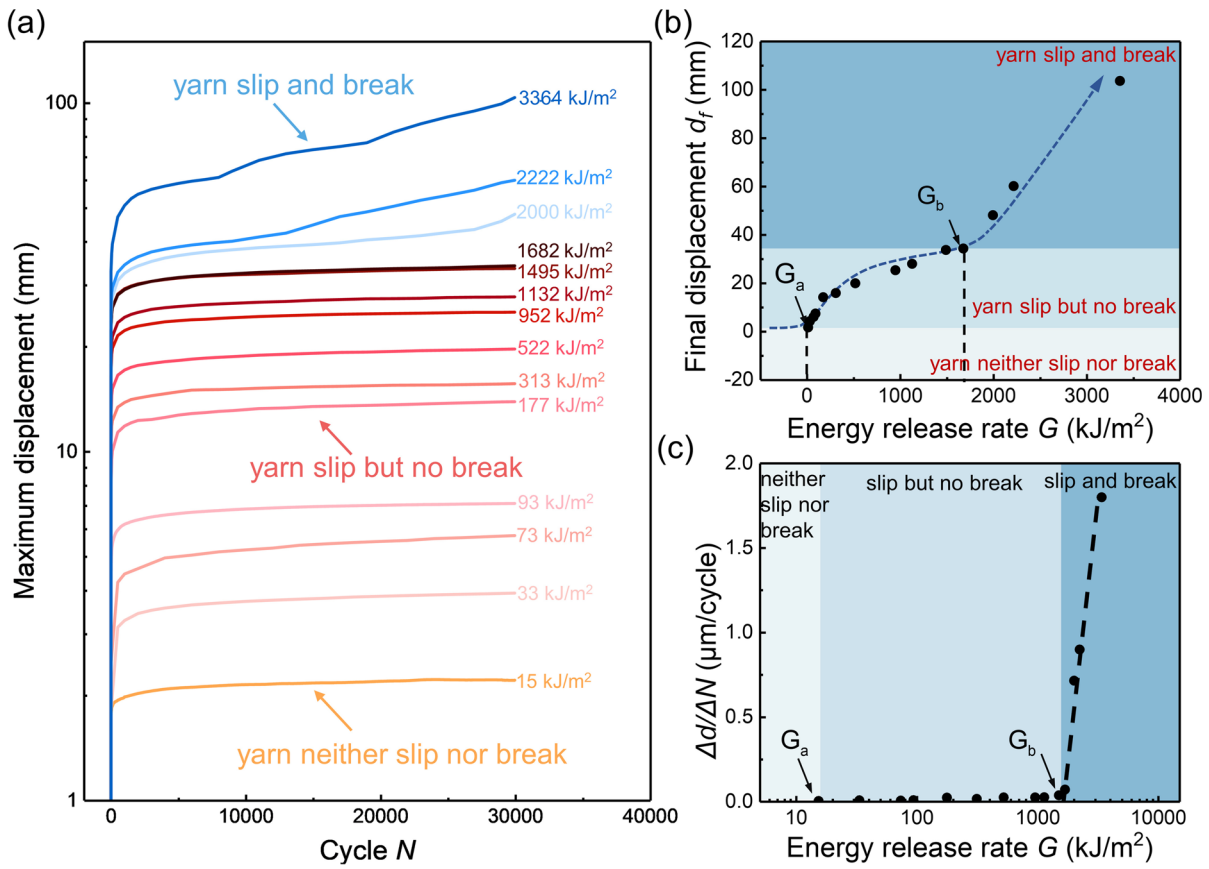

Fig. 5 Displacement in the composite. **a** The maximun displacement over cycles for different amplitudes of energy release rate G. **b** The final displacement d_f as a function of G. **c** The displacement per cycle $\Delta d/\Delta N$ as a function of G

average peak tear force of the composite with weak interface is higher than that of strong interface. For the composite with strong interface, the force–displacement curve is zig-zag, caused by periodical sliding and breaking of the warp yarns (Fig. 8b). For the composite with weak interface, the force–displacement curve is smooth, and the specimen tears by yarn sliding (Fig. 8c).

5 Tearing of the composite with a strong interface under cyclic load

We tear a specimen of the composite with a strong interface using cyclic force of a fixed amplitude, and record the maximum displacement d as a function of the number of cycles N. The experiment is repeated for various amplitudes of energy release rate (Fig. 9a). We calculate the maximum displacement growth per cycle $\Delta d/\Delta N$ and final maximum displacement d_f as a function of energy release rate G (Fig. 9b, c). The behavior for the fatigue crack growth is similar to the composite with a weak interface. When $G > G_b$, the yarns at the crack tip slip and break. The crack grows continuously. The displacement per cycle $\Delta d/\Delta N$ increases with G. When $G_a < G < G_b$, the crack propagates initially by yarn slip without yarn break, and arrests eventually. When $G < G_a$, the yarns at the crack tip do not slip or break. For this composite with a strong interface, our test gives the values of the two thresholds: G_a = 36 kJ/m^2 and G_b = 747 kJ/m^2.

We compare G_a and G_b for the composites with weak interface and strong interface. G_a increases with the interface strength (Fig. 10a), while G_b decreases with the interface strength (Fig. 10b). G_a is the threshold below which the yarn does not slip. For the strong interface, the resistance to fiber slippage is higher than the weak interface, hence G_a is increased.

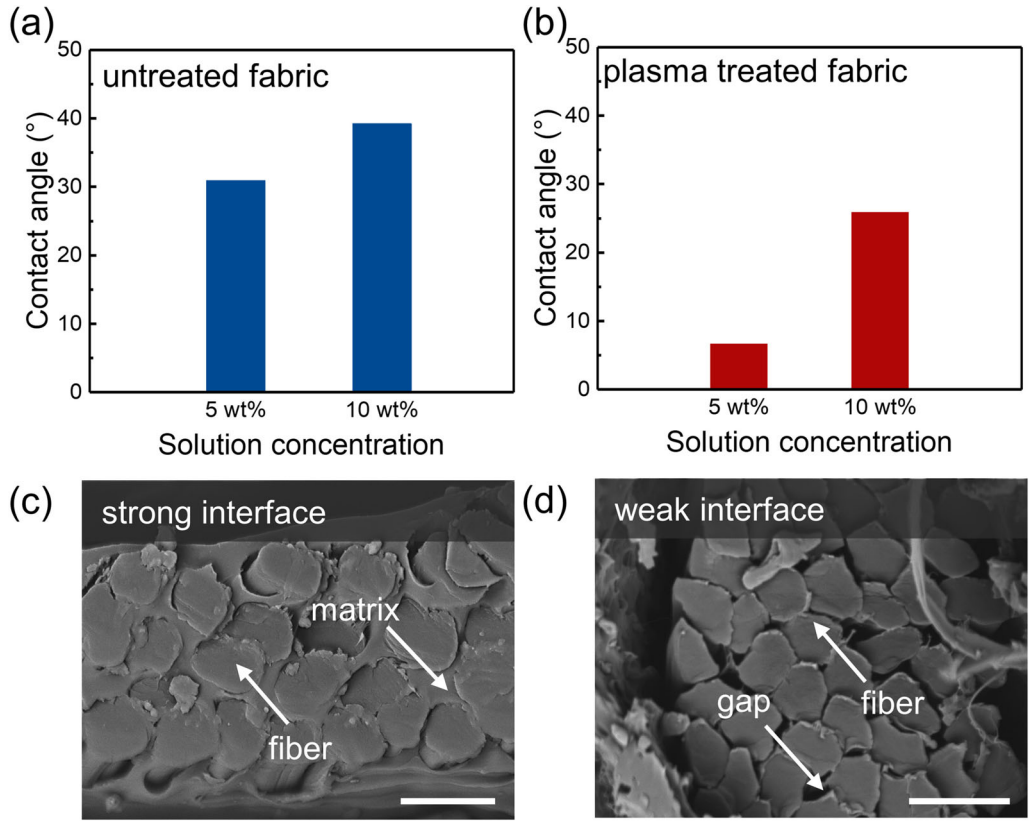

Fig. 6 Strengthening of the interface by plasma-treating the fabric and diluting the TPU solution. The contact angle of the TPU solution on the **a** untreated fabric and **b** plasma treated fabric changes with concentration of the solution. SEM images of the cross sections of the composites with **c** plasma treated fabric and 5 wt% TPU solution, and **d** untreated fabric and 10 wt% TPU solution. Scale bar is 25 μm

G_b is the threshold for continuous crack growth by yarn breaking. The strong interface limits yarn slippage, and leads to a higher stress concentration at the crack tip than the case of weak interface. When the stress reaches the endurance stress of the fiber, fiber breaks. For the same fiber, the yarns will break prematurely in the composite with a strong interface, thus G_b is decreased. Both G_a and G_b of the composite are much higher than existing soft materials, whose fatigue thresholds are $10^{-3} \sim 1$ kJ/m^2 (Zhao et al. 2021). Such extraordinary fatigue resistance is due to the macro fiber length and strong fiber strength. High-strength long fibers allow the yarn to slide, which reduces the stress concentration at the crack tip and yields a high fatigue threshold.

6 Discussion

When $G < G_a$, we do not observe crack growth. When $G_a < G < G_b$, crack growth and arrest are observed. As the crack grows, the yarns are jammed to form the delta-shaped zone at the wake of the crack tip. The yarns do not break, but bridge the crack (Fig. 11a). We measure the bridging zone size, b, as a function of the amplitude of energy release rate, G (Fig. 11b). The maximum bridging zone size is 19 mm for the composites with weak interface, and 8 mm for the composite with strong interface. When $G > G_b$, yarns break, and the bridging zone propagates. The relation between the bridging zone size and the amplitude of energy release rate, which is measured under cyclic load, is analogous to the crack resistance curve commonly reported for materials under monotonic load. Thus, the b-G curves may be regarded as crack resistance curves under cyclic load.

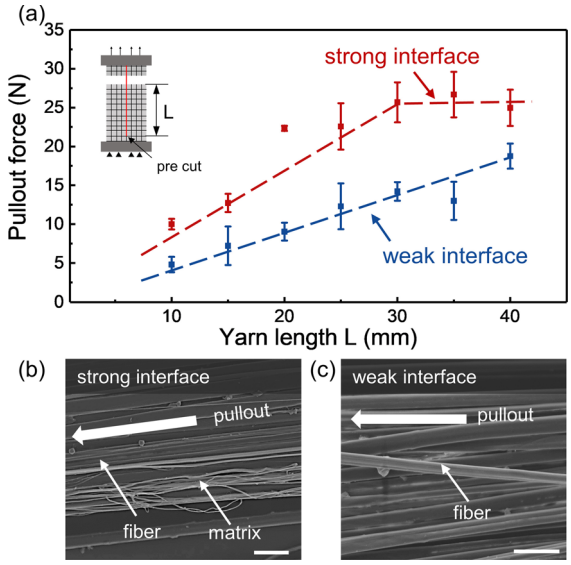

Fig. 7 Pulling out of a single yarn from the composite. **a** Maximum pullout force as a function of the yarn length. SEM image of the yarn pulled out from the composite with **b** a strong interface and **c** a weak interface. Scale bar is 50 μm

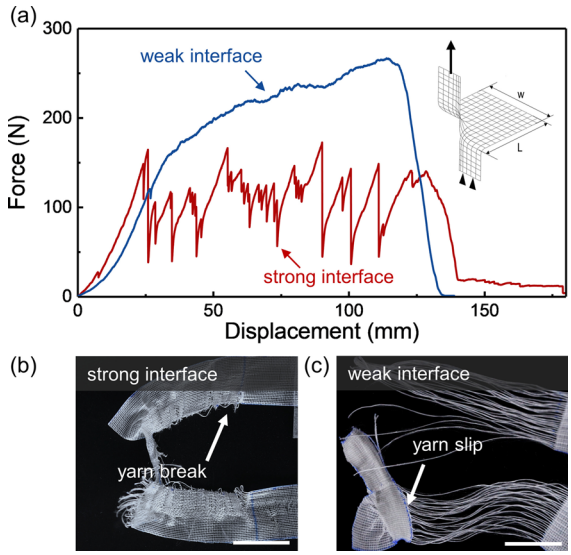

Fig. 8 Tearing of the composite under monotonic load. **a** Force–displacement curves of the composites with strong and weak interfaces. **b** The composite with a strong interface tears by yarn breaking. **c** The composite with a weak interface tears by yarn sliding. Scale bar is 20 mm

A similar phenomenon exists for fatigue crack growth in metals and ceramic-matrix composites (Tanaka and Nakai 1983; Zerbst et al. 2016). In such a test of a material, a single specimen with a precrack is cyclically loaded by increasing the amplitudes of force (Tabernig and Pippan 2002). The test also identifies two thresholds, called the short-crack threshold and long-crack threshold. The merit of such a test is that a single specimen generates the entire crack-resistance curve under cyclic load. However, these experiments often use a specimen with a very short precut crack. Consequently, the resistance curve reported is expected to be sensitive to the length of the precrack. By contrast, in our experiment, the precrack length exceeds the largest bridging zone length, so that the resistance curves are expected to be *insensitive* to the length of the precrack. Furthermore, because the legs are nearly inextensible, the maximum displacement is about twice the bridging zone size. Thus, the d_f–G curves may as well be used as the crack resistance curves under cyclic load. This method eliminates the need to measure crack growth.

Two thresholds are also identified for a polyampholyte hydrogel with hierarchical structure of sparse/dense domain (Li et al. 2020b). The first threshold is related to the break of single polymer chains ($\sim$ 10 nm), and the second threshold is related to the break of dense polymer domains ($\sim$ 100 nm). Homogeneous soft materials only show one threshold, including natural rubber (Lake and Thomas 1967), polyacrylamide hydrogel (Tang et al. 2017), tough hydrogel (Bai et al. 2017) and double network hydrogel (Zhang et al. 2018). The threshold is due to scission of the polymer chains lying across the crack plane. Furthermore, both the two fatigue thresholds and the bridging zone size are also influenced by the fabric structure (e.g. yarn thickness, yarn density, fabric weaving method). The effect of these parameters on the fatigue properties of the composite is worthwhile to investigate in the future.

7 Conclusion

In this work, we fabricate a composite of UHMWPE woven fabric and TPU matrix, and cyclically tear the composite under energy release rate of a fixed amplitude, G. The composite exhibits two fatigue thresholds. The yarn slip determines the first fatigue threshold G_a for the initiation of fatigue crack growth. After crack initiates, yarns jam behind the crack tip to form a bridging zone, and the crack arrests until reaching the second threshold G_b. Above G_b, the crack

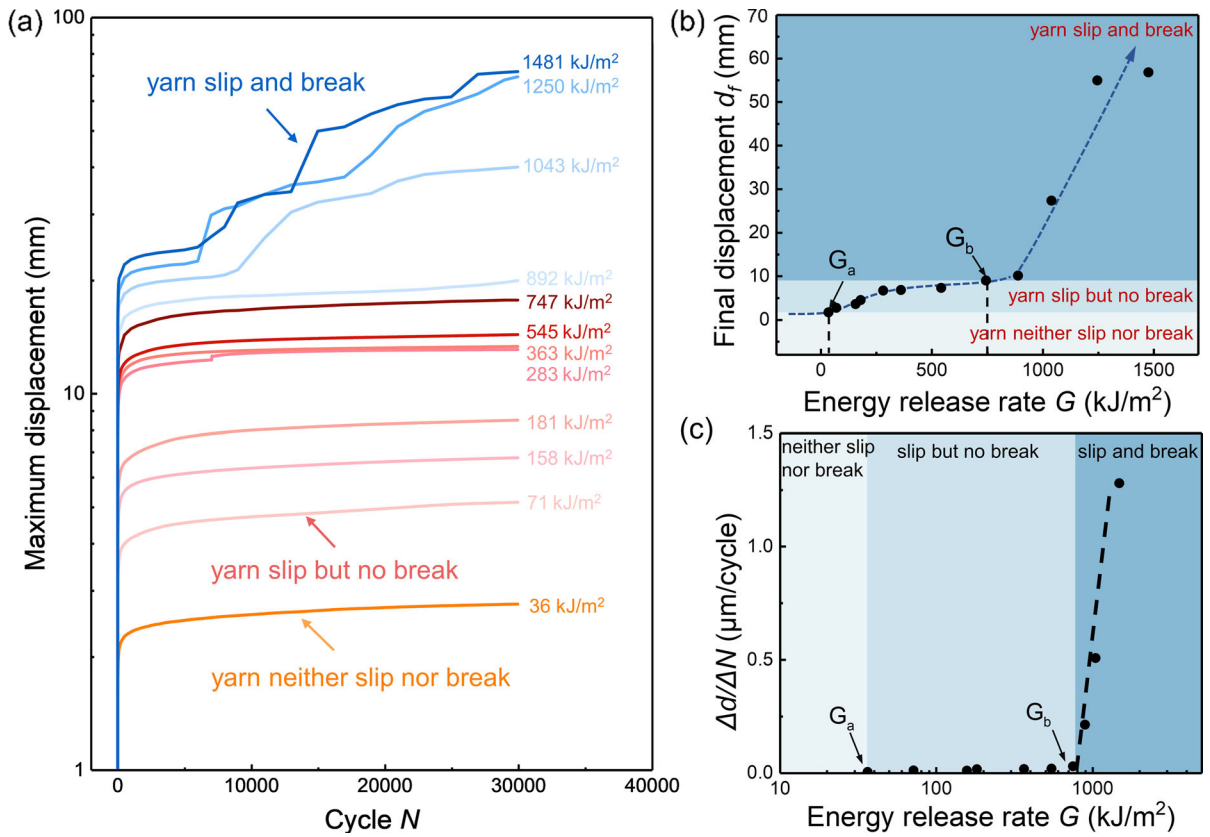

Fig. 9 Displacement in the composite with a strong interface. **a** The maximum displacement over cycles for different amplitudes of energy release rate G. **b** The final maximum displacement d_f as a function of G. **c** The displacement per cycle $\Delta d/\Delta N$ as a function of G

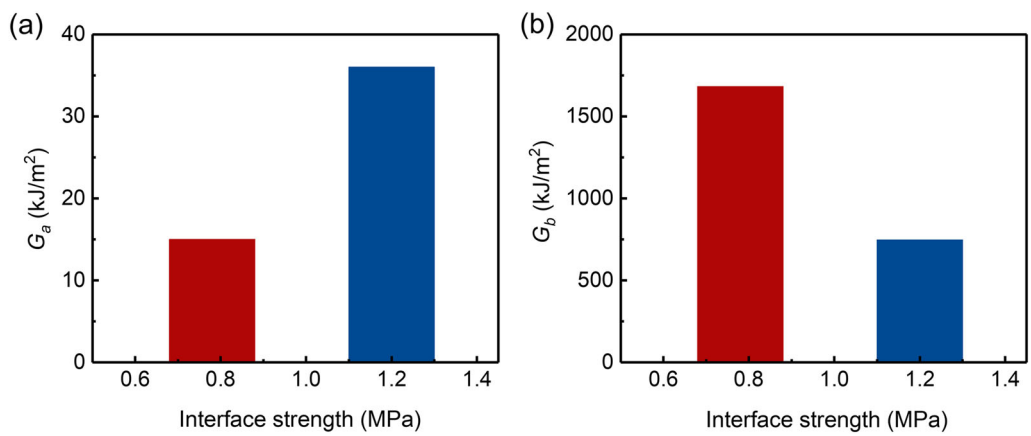

Fig. 10 Two thresholds **a** G_a and **b** G_b, for the composites with strong and weak interfaces

grows continuously by yarn slip and yarn break. The interface strength affects the fatigue crack growth in the composite. We find that G_a is increased by strengthening the interface, while G_b is decreased. Furthermore, a bridging zone of several millimeters forms during the crack propagation. This large bridging zone is related to the fabric structure. This work may guide the design of fatigue resistant composites.

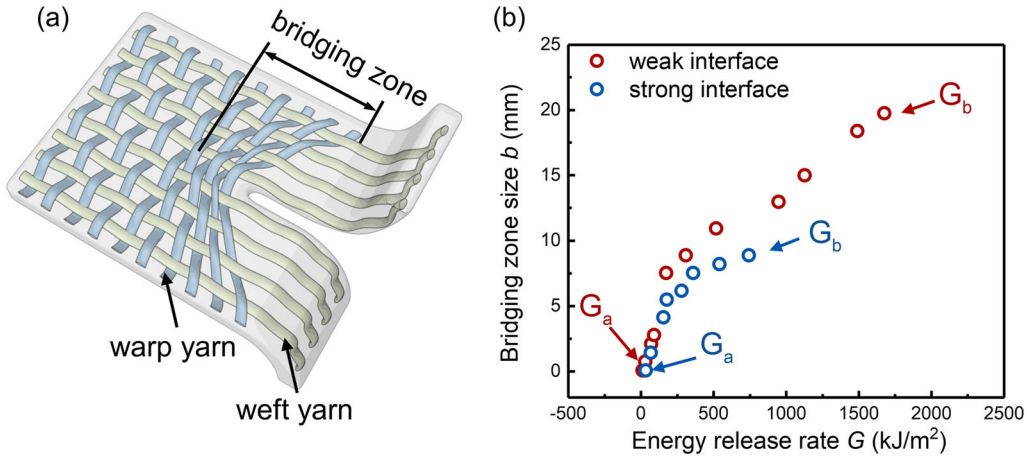

Fig. 11 Comparison of the bridging zone size for the composites with strong and weak fabric/matrix interfaces. **a** Schematic of the bridging zone formed during cyclic loading. **b** The bridging zone size b of the composite as a function of the amplitude of energy release rate G

Acknowledgements This research was supported by the National Natural Science Foundation of China (Grant No. 12422204). JD.T. acknowledges the support of K. C. Wong Education Foundation.

Author contributions Conceptualization: JYT, ZGS, JDT. Methodology: JYT, XC, FKL, ZGS, JDT. Formal analysis and investigation: JYT, XC, FKL, ZGS, JDT. Writing—original draft preparation: JYT, JDT. Writing—review and editing: ZGS, JDT. Supervision: ZGS, JDT.

Data availability No datasets were generated or analysed during the current study.

Declarations

Conflict of interest The authors declare that they have no conflict of interest.

References

Bai R, Yang Q, Tang J et al (2017) Fatigue fracture of tough hydrogels. Extreme Mech Lett 15:91–96. https://doi.org/10.1016/j.eml.2017.07.002

Bresciani L, Manes A, Giglio M (2015) An analytical model for ballistic impacts against plain-woven fabrics with a polymeric matrix. Int J Impact Eng 78:138–149. https://doi.org/10.1016/j.ijimpeng.2015.01.001

Cui W, King DR, Huang Y et al (2020) Fiber-reinforced viscoelastomers show extraordinary crack resistance that exceeds metals. Adv Mater 32:1907180. https://doi.org/10.1002/adma.201907180

Cui W, Huang Y, Chen L et al (2021) Tiny yet tough: maximizing the toughness of fiber-reinforced soft composites in the absence of a fiber-fracture mechanism. Matter 4:3646–3661. https://doi.org/10.1016/j.matt.2021.08.013

Ghanavaty AM, Mosalmani R, Shishesaz M (2024) Progressive damage analysis for fatigue life prediction in plain weave composites: a multi-scale approach. J Compos Mater 58:343–359. https://doi.org/10.1177/00219983231218783

He Y, Zhao XY, Rao P et al (2022) Saline tolerant tough-yet-strong fiber-reinforced gel-nacre for soft actuator. Chem Eng J 446:137091. https://doi.org/10.1016/j.cej.2022.137091

Huang Y, King DR, Sun TL et al (2017) Energy-dissipative matrices enable synergistic toughening in fiber reinforced soft composites. Adv Func Mater 27:1605350. https://doi.org/10.1002/adfm.201605350

Huang Y, King DR, Cui W et al (2019) Superior fracture resistance of fiber reinforced polyampholyte hydrogels achieved by extraordinarily large energy-dissipative process zones. J Mater Chem A 7:13431–13440. https://doi.org/10.1039/C9TA02326G

Kim J-K, Sham M-L (2000) Impact and delamination failure of woven-fabric composites. Compos Sci Technol 60:745–761. https://doi.org/10.1016/S0266-3538(99)00166-9

King DR, Sun TL, Huang Y et al (2015) Extremely tough composites from fabric reinforced polyampholyte hydrogels. Mater Horiz 2:584–591. https://doi.org/10.1039/C5MH00127G

Kumar SM, Ravikiran KR, Govindaraju H (2018) Development of E-glass woven fabric/polyester resin polymer matrix composite and study of mechanical properties. Mater Today Proc 5:13367–13374. https://doi.org/10.1016/j.matpr.2018.02.329

Lake GJ, Thomas AG (1967) The strength of highly elastic materials. Proc R Soc Lond A 300:108–119. https://doi.org/10.1098/rspa.1967.0160

Li C, Yang H, Suo Z, Tang J (2020a) Fatigue-resistant elastomers. J Mech Phys Solids 134:103751. https://doi.org/10.1016/j.jmps.2019.103751

Li X, Cui K, Sun TL et al (2020b) Mesoscale bicontinuous networks in self-healing hydrogels delay fatigue fracture.

Proc Natl Acad Sci 117:7606–7612. https://doi.org/10.1073/pnas.2000189117

Liao I-C, Moutos FT, Estes BT et al (2013) Composite three-dimensional woven scaffolds with interpenetrating network hydrogels to create functional synthetic articular cartilage. Adv Func Mater 23:5833–5839. https://doi.org/10.1002/adfm.201300483

Liu F, Suo Z, Tang J (2022a) How does a glass fabric tear under cyclic force? J Mech Phys Solids 158:104659. https://doi.org/10.1016/j.jmps.2021.104659

Liu X, Wu J, Qiao K et al (2022b) Topoarchitected polymer networks expand the space of material properties. Nat Commun 13:1622. https://doi.org/10.1038/s41467-022-29245-0

Pandita SD, Huysmans G, Wevers M, Verpoest I (2001) Tensile fatigue behaviour of glass plain-weave fabric composites in on- and off-axis directions. Compos Part A Appl Sci Manuf 32:1533–1539. https://doi.org/10.1016/S1359-835X(01)00053-7

Patti A, Costa F, Perrotti M et al (2021) Polyurethane impregnation for improving the mechanical and the water resistance of polypropylene-based textiles. Materials 14:1951. https://doi.org/10.3390/ma14081951

Rajak DK, Wagh PH, Linul E (2022) A review on synthetic fibers for polymer matrix composites: performance, failure modes and applications. Materials 15:4790. https://doi.org/10.3390/ma15144790

Sevenois R, Van Paepegem W (2015) Fatigue damage modeling techniques for textile composites: review and comparison with unidirectional composite modeling techniques. Appl Mech Rev 67:020802. https://doi.org/10.1115/1.4029691

Sharabi M (2022) Structural mechanisms in soft fibrous tissues: a review. Front Mater 8:793647. https://doi.org/10.3389/fmats.2021.793647

Szczesny SE, Fetchko KL, Dodge GR, Elliott DM (2017) Evidence that interfibrillar load transfer in tendon is supported by small diameter fibrils and not extrafibrillar tissue components. J Orthop Res 35:2127–2134. https://doi.org/10.1002/jor.23517

Tabernig B, Pippan R (2002) Determination of the length dependence of the threshold for fatigue crack propagation. Eng Fract Mech 69:899–907. https://doi.org/10.1016/S0013-7944(01)00129-1

Tanaka K, Nakai Y (1983) Propagation and non-propagation of short fatigue cracks at a sharp notch. Fatigue Fract Eng Mater Struct 6:315–327. https://doi.org/10.1111/j.1460-2695.1983.tb00347.x

Tang J, Li J, Vlassak JJ, Suo Z (2017) Fatigue fracture of hydrogels. Extreme Mech Lett 10:24–31. https://doi.org/10.1016/j.eml.2016.09.010

Taylor HM (1959) 9—tensile and tearing strength of cotton cloths. J Text Inst Trans 50:T161–T188. https://doi.org/10.1080/19447025908662490

Thomas A (1994) The development of fracture mechanics for elastomers. Rubber Chem Technol 67:50–67. https://doi.org/10.5254/1.3538688

Triki E, Dolez P, Vu-Khanh T (2011) Tear resistance of woven textiles—criterion and mechanisms. Compos B Eng 42:1851–1859. https://doi.org/10.1016/j.compositesb.2011.06.015

Triki E, Vu-Khanh T, Nguyen-Tri P, Boukehili H (2012) Mechanics and mechanisms of tear resistance of woven fabrics. Theoret Appl Fract Mech 61:33–39. https://doi.org/10.1016/j.tafmec.2012.08.004

Vesely I (1997) The role of elastin in aortic valve mechanics. J Biomech 31:115–123. https://doi.org/10.1016/S0021-9290(97)00122-X

Wang Z, Xiang C, Yao X et al (2019) Stretchable materials of high toughness and low hysteresis. Proc Natl Acad Sci 116:5967–5972. https://doi.org/10.1073/pnas.1821420116

Xiang C, Wang Z, Yang C et al (2020) Stretchable and fatigue-resistant materials. Mater Today 34:7–16. https://doi.org/10.1016/j.mattod.2019.08.009

Yang H, Ji M, Yang M et al (2021) Fabricating hydrogels to mimic biological tissues of complex shapes and high fatigue resistance. Matter 4:1935–1946. https://doi.org/10.1016/j.matt.2021.03.011

Zeng L, Liu F, Yu Q et al (2023) Flaw-insensitive fatigue resistance of chemically fixed collagenous soft tissues. Sci Adv 9:eade7375. https://doi.org/10.1126/sciadv.ade7375

Zerbst U, Vormwald M, Pippan R et al (2016) About the fatigue crack propagation threshold of metals as a design criterion—a review. Eng Fract Mech 153:190–243. https://doi.org/10.1016/j.engfracmech.2015.12.002

Zhang W, Liu X, Wang J et al (2018) Fatigue of double-network hydrogels. Eng Fract Mech 187:74–93. https://doi.org/10.1016/j.engfracmech.2017.10.018

Zhang G, Yin T, Nian G, Suo Z (2021) Fatigue-resistant polyurethane elastomer composites. Extreme Mech Lett 48:101434. https://doi.org/10.1016/j.eml.2021.101434

Zhao X, Chen X, Yuk H et al (2021) Soft materials by design: unconventional polymer networks give extreme properties. Chem Rev 121:4309–4372. https://doi.org/10.1021/acs.chemrev.0c01088